Oxidation of Fatty Acids Is the Source of Increased Mitochondrial Reactive Oxygen Species Production in Kidney Cortical Tubules in Early Diabetes

Mariana G. Rosca,[1,2] Edwin J. Vazquez,[3,4] Qun Chen,[5] Janos Kerner,[1,2] Timothy S. Kern,[2,6] and Charles L. Hoppel[1,2,6]

Mitochondrial reactive oxygen species (ROS) cause kidney damage in diabetes. We investigated the source and site of ROS production by kidney cortical tubule mitochondria in streptozotocin-induced type 1 diabetes in rats. In diabetic mitochondria, the increased amounts and activities of selective fatty acid oxidation enzymes is associated with increased oxidative phosphorylation and net ROS production with fatty acid substrates (by 40% and 30%, respectively), whereas pyruvate oxidation is decreased and pyruvate-supported ROS production is unchanged. Oxidation of substrates that donate electrons at specific sites in the electron transport chain (ETC) is unchanged. The increased maximal production of ROS with fatty acid oxidation is not affected by limiting the electron flow from complex I into complex III. The maximal capacity of the ubiquinol oxidation site in complex III in generating ROS does not differ between the control and diabetic mitochondria. In conclusion, the mitochondrial ETC is neither the target nor the site of ROS production in kidney tubule mitochondria in short-term diabetes. Mitochondrial fatty acid oxidation is the source of the increased net ROS production, and the site of electron leakage is located proximal to coenzyme Q at the electron transfer flavoprotein that shuttles electrons from acyl-CoA dehydrogenases to coenzyme Q. *Diabetes* **61:2074–2083, 2012**

Diabetic nephropathy (DN) is the leading cause of end-stage renal disease (ESRD) (1). Hyperlipidemia is an independent factor in renal injury in animals (2) and humans (3). Increased fatty acid (FA) synthesis enzymes and triglyceride deposition correlated with increased profibrotic factors were found in the kidney in diabetes in rats (4) and mice (5). Inhibition of lipid synthesis in humans (6) and amelioration of dyslipidemia (7) protect against diabetic renal disease.

Glomerular disease has been considered the initial and cardinal manifestation of DN. However, tubulointerstitial fibrosis is considered a strong predictor of the progressive loss of renal function leading to ESRD (8,9) and has been shown to determine the progression to ESRD (10).

The increase in plasma nonesterified FAs (NEFAs) is a major component of diabetic dyslipidemia. Tubular cells are exposed to blood and urine FAs present in free form or bound to albumin. The expression of cluster of differentiation 36 (CD36) involved in the transport of FA is induced by high glucose in proximal tubular cells and causes palmitate-induced apoptosis only in human kidneys with diabetic tubular epithelial degeneration (11). Albumin-bound FA, rather than albumin, itself is a major mediator of tubulointerstitial lesions in various types of proteinuria-developing ESRD (12,13).

Proximal tubular cells (>90% of the kidney cortex) engage in active uptake and transepithelial transport of glucose, but only a small amount of glucose, if any, is used for ATP production (14). Moreover, diabetes causes a decrease in kidney glucose oxidation due to the inhibition of pyruvate dehydrogenase activity (15). Skin fibroblasts isolated from type 1 diabetic patients, with very fast rates in developing DN, have increased expression of genes involved in mitochondrial FA oxidation (16). The data suggest an energy fuel preference in diabetes favoring fat oxidation at the expense of glycolysis. The enzyme carnitine palmitoyltransferase 1 (CPT1) catalyzes the rate-controlling step in the overall mitochondrial FA β-oxidation pathway. Its expression is reported to be increased in liver and heart in diabetes, whereas its sensitivity to malonyl-CoA is reduced, favoring its activity.

Increased generation of ROS within the mitochondrial electron transport chain (ETC) has been considered to be an important contributor to the development of chronic diabetes complications (17). Increased availability of glucose-generated reducing equivalents in cultured aortic endothelial (18) and retinal (19) cells or defects in the ETC in epineural (20) and cardiac (21) mitochondria increase the electron pressure at specific mitochondrial sites. This perturbation prolongs the lifetime of partially reduced intermediates that donate electrons to molecular oxygen to form superoxide. In contrast, although mitochondrial-targeted antioxidant mitoquinone mesylate (mitoQ) is beneficial in the treatment of diabetic nephropathy, mitochondrial ETC is not the source of ROS generation in the kidney of diabetic Akita mice (22) or in the sensory neurons from diabetic rats (23), indicating that there are differences in the source and sites of ROS production in target organs of diabetes complications. In short-term diabetes, we found that mitochondrial ETC is neither the target nor the site of ROS generation in kidney cortical tubules. The source of increased ROS production is mitochondrial FA β-oxidation; the site of electron leakage is located proximal to CoQ at the electron transfer flavoprotein that shuttles electrons from acyl-CoA dehydrogenases to coenzyme Q.

RESEARCH DESIGN AND METHODS

Reagents. Unless otherwise specified, all reagents were purchased from Sigma-Aldrich (St. Louis, MO) and were of the highest purity grade.

Animal model. The investigation conforms to the *Guide for the Care and Use of Laboratory Animals* (U.S. National Institutes of Health Publication No. 85-23, revised 1996). All experimental protocols were approved by the Case Western Reserve University institutional animal care and use committees. Diabetes was induced by intraperitoneal injection of streptozotocin (55 mg/kg of body weight) in citrate buffer to 12-h fasted male Wistar rats. Two units of NPH insulin were given subcutaneously thrice weekly to avoid severe hypercatabolic state. Glycated hemoglobin was measured by affinity chromatography of the intracardiac blood.

Quantification of serum NEFA and triglyceride-bound glycerol. The concentration of serum NEFA and of triglyceride-bound glycerol was determined using gas chromatography-electron impact ionization mass spectrometry, as described by Bederman et al. (24). Palmitate, stearate, and oleate were analyzed as trimethylsilyl derivatives and quantified against a known amount of heptadecanoic acid. Serum triglyceride-bound glycerol was quantified as a triacetate derivative after an alkaline hydrolysis procedure and the addition of a known amount of internal standard of deuterium-labeled glycerol.

Isolation of tubule mitochondria. The kidneys cortices were separated from the medulla. Glomeruli were first isolated (25), and the material consisting of tubulointerstitium was collected in buffer A (220 mmol/L mannitol, 70 mmol/L sucrose, 5 mmol/L 3-(N-morpholino)propanesulfonic acid [MOPS], 10 mmol/L EGTA, 0.2% BSA, pH 7.4). Phase-contrast microscopy was performed during each experiment to examine the purity of the glomerular material and ensure that the entire tubular population was harvested within the tubulointerstitial material. Because the tubules represent the major component of the cortical tubulointerstitial material, the isolated mitochondria were designated as cortical tubule mitochondria. Tubule mitochondria were isolated (26) and suspended in buffer B (100 mmol/L KCl, 50 mmol/L MOPS, and 0.5 mmol/L EGTA, pH 7.4).

Oxidative phosphorylation. Oxygen consumption was measured with a Clark-type electrode (Strathkelvin) in respiration buffer (100 mmol/L KCl, 50 mmol/L MOPS, 1 mmol/L EGTA, 5 mmol/L KH_2PO_4, and 1 mg/mL defatted BSA, pH 7.4) (27) at 30°C with glutamate (20 mmol/L) + malate (5 mmol/L), pyruvate (10 mmol/L) + malate, succinate (20 mmol/L) + rotenone (3.75 μmol/L), durohydroquinone (DHQ, 1 mmol/L) + rotenone, N,N,N',N'-tetramethyl-p-phenylenediamine (TMPD) + ascorbate (1:10 mmol/L) + rotenone, palmitoyl-CoA (0.02 mmol/L) + carnitine (2 mmol/L) + malate, and palmitoylcarnitine (0.04 mmol/L) or octanoylcarnitine (0.2 mmol/L) + malate, as substrates. State 3 respiration rate, which is ADP-dependent was measured with 200 μmol/L ADP. State 4 respiration (ADP-limited) was recorded after ADP consumption. Then, sequential additions of 2 mmol/L ADP and 200 μmol/L of the uncoupler dinitrophenol were made to determine the maximal ADP-stimulated and uncoupled respiratory rates, respectively. State 3-to-state 4 respiratory control ratios (RCR) reflect the control of oxygen consumption by phosphorylation ("coupling"). The ADP-to-oxygen ratio (number of ADP molecules added for each oxygen atom consumed) (28) is an index of the efficiency of oxidative phosphorylation. In preliminary experiments, the complex IV inhibitor sodium azide (400 μmol/L) completely inhibited oxidative phosphorylation with complex IV substrates in both control and diabetic tubule mitochondria, showing that the azide-sensitive complex IV–supported respiration equals the TMPD + ascorbate–supported respiration and that there are no differences in azide sensitivity between control and diabetic tubule mitochondria. Therefore, the results are presented as TMPD + ascorbate–supported respiration. Rates of oxygen consumption are expressed in nano atoms (nA) oxygen per minute per milligram of mitochondrial proteins.

Measurement of CPT1 activity. The activity of CPT1 was determined using the modified radiochemical forward assay by measuring the formation of ^{14}C-labeled palmitoylcarnitine from ^{14}C-carnitine and palmitoyl-CoA at 37°C as described (29). CPT1 activity was expressed as the activity inhibited by 200 μmol/L malonyl-CoA and given in nanomoles per minute per milligram of protein. Malonyl-CoA sensitivity was determined at fixed palmitoyl-CoA concentrations by varying the concentration of malonyl-CoA.

Measurement of fatty acid oxidation enzymes. Frozen-thawed mitochondria were treated with 0.5% cholate and diluted to 0.1 mg/mL buffer A. The dehydrogenase assays used octanoyl-CoA for medium-chain acyl-CoA dehydrogenase (MCAD) and palmitoyl-CoA for long-chain acyl-CoA dehydrogenase (LCAD) with phenazine ethosulfate as an intermediate electron acceptor from flavin adenine dinucleotide ($FADH_2$) and oxidized cytochrome c as the final electron acceptor. The reduction of cytochrome c was recorded spectrophotometrically at 550 nm.

Western blot analysis. Proteins (equal amounts of kidney tubule mitochondrial protein [18 μg/lane], heart mitochondrial protein [6.5 μg/lane], and liver outer membrane protein [0.5 μg/lane]) were subjected to SDS-PAGE,

electroblotted onto polyvinylidene fluoride membranes, and probed with specific antibodies. Densitometric evaluation of the gels was carried out using ImageJ software (National Institutes of Health) coupled with Multi Gauge V3.0 (Fujifilm Life Science).

The antibodies used in this study were as follows: liver (^{620}MDPKSTAEQRLK^{631}) and liver + muscle (^{230}NYVSDWWEEYIYLRGR^{245}) isoforms of CPT1 (30) at 1:3000 dilutions in overnight incubations; beef liver mitochondrial CPT2 (29), carnitine acyl-carnitine translocase (CACT) (31), MCAD (Epitomics) at 1:3000 dilutions, each in 2-h successive incubations; manganese superoxide dismutase (Mn-SOD) and copper/zinc SOD (Cu/Zn-SOD; Assay Designs) at 1:5000 dilutions in overnight incubations. All membranes were stripped and incubated with iron sulfur protein antibody (MitoSciences) as a loading control at 1:5000 dilution overnight. The amount of this protein is unchanged in kidney mitochondria in type 1 diabetes (32). Secondary antibodies (BioRad) were used at 1:10000 dilutions in 1 h incubation. Multiple exposure times were used for developing, and the optimal ones were chosen for presentation.

Measurement of hydrogen peroxide (H_2O_2) produced by mitochondria. The production of ROS by intact mitochondria was measured as the rate of oxidation of the fluorogenic indicator, Amplex red, by H_2O_2 in the presence of horseradish peroxidase (33). H_2O_2 production was initiated by substrates in concentrations similar to those indicated for oxidative phosphorylation measurements. Rotenone and antimycin A were added to inhibit the activities of complex I and III, respectively. Fluorescence was recorded in a microplate reader with 530-nm excitation and 590-nm emission wavelengths. Standard curves with known amounts of H_2O_2 were linear up to 2 μmol/L H_2O_2. The rate of H_2O_2 production also was linear with respect to mitochondrial protein. The results are presented as fluorescence in the presence of mitochondria minus the background (absence of mitochondria) in picomoles of H_2O_2 per milligram of mitochondrial protein/30 min.

Statistical analysis. The results were analyzed using the Student two-tailed two-sample t test. Data are reported as mean ± SEM. $P < 0.05$ was considered significant.

RESULTS

Clinical and biochemical characteristics of diabetic rats. Diabetic rats did not lose weight during the study but showed decreased weight gain, hyperglycemia, polyuria, and increased glycated hemoglobin levels 8–9 weeks after the onset of diabetes (Table 1). The serum was macroscopically turbid, indicating secondary diabetic hyperlipidemia. Glycerol and NEFA levels were increased in sera of diabetic rats compared with the control rats. Kidney weight was significantly increased in the diabetic group, suggesting renal hypertrophy. Mitochondrial yield does not change in diabetes (20.1 ± 2.9 vs. 18.9 ± 1.2 mg mitochondrial protein/g wet cortex tissue in control and diabetic

TABLE 1

Clinical and biochemical characteristics of control and diabetic rats

	Control rats ($n = 7$)	Diabetic rats ($n = 6$)
Study duration (weeks)	9.0 ± 1.6	8.0 ± 1.0
Body weight (g)		
Beginning of the study	310 ± 12	275 ± 15
End of the study	410 ± 24	320 ± 37*
Glycemia (mg/100 mL)	142.5 ± 10.5	255.1 ± 4.5*
HbA$_{1c}$ (%)	2.9 ± 0.1	9.7 ± 0.3*
Serum visual appearance	Clear	Turbid
Glycerol (mmol/L)	2.114 ± 0.169	19.208 ± 2.109*
Total NEFA (mmol/L)	0.370 ± 0.007	1.256 ± 0.131*
Palmitic acid (mmol/L)	0.156 ± 0.003	0.490 ± 0.046*
Oleic acid (mmol/L)	0.095 ± 0.004	0.421 ± 0.046*
Stearic acid (mmol/L)	0.119 ± 0.008	0.345 ± 0.034*
Kidney weight (g)	1.5 ± 0.0	1.8 ± 0.1*
Diuresis (mL/day)	11.8 ± 1.5	153.0 ± 3.6*

Data are presented as mean ± SEM. *$P < 0.05$.

tubules, respectively), suggesting that there has been no change in mitochondrial content in kidney tubules.

Substrate processing rather than the mitochondrial ETC is changed in kidney tubules in diabetes. Diabetic tubule kidney mitochondria oxidizing glutamate have higher state 3 respiratory rates compared with the control (Table 2). The ADP-to-oxygen ratios were unchanged, showing that the coupling efficiency of the tubule kidney mitochondria is preserved in diabetes. With the uncoupler, dinitrophenol, the glutamate-supported respiratory rates of nondiabetic tubule mitochondria do not increase nor do they reach the level of respiratory rates of diabetic mitochondria (Table 2). The oxidation of glutamate + malate is not changed by diabetes in tubule mitochondria, whereas pyruvate + malate oxidation is lower in diabetic tubule mitochondria compared with the control (Fig. 1A). The oxidation of succinate, which donates electrons to FAD in complex II, was unchanged in diabetic tubule mitochondria, as were the state 3 respiratory rates with durohydroquinone (complex III electron donor) and those with the cytochrome c electron donor TMPD + ascorbate (Fig. 1A). The data show that the ETC complexes in tubule mitochondria are not the targets of diabetes-induced alterations in this experimental model.

Mitochondrial FA oxidation is increased in kidney tubules in diabetes. CPT1 is the rate-controlling enzyme in mitochondrial FA oxidation. We measured oxidative phosphorylation rates with CPT1-dependent and CPT1-independent substrates. Palmitoyl-CoA is converted to palmitoylcarnitine by the outer membrane CPT1. Palmitoylcarnitine and octanoylcarnitine are transported into the mitochondrial matrix via the CACT bypassing CPT1, and react with CoA in the matrix in a reaction catalyzed by the inner membrane CPT2. Within the matrix, palmitoyl-CoA and octanoyl-CoA undergo sequential β oxidation, producing acetyl-CoA, NADH, and $FADH_2$. Electrons from NADH enter the ETC at complex I, whereas those from the $FADH_2$ of acyl-CoA dehydrogenases enter the ETC at complex III via electron transfer flavoprotein (ETF) and ETF-coenzyme Q oxidoreductase (ETF-QOR). As shown in Fig. 1B, CPT1-dependent and CPT1-independent lipid substrates were both oxidized at higher rates by diabetic tubule mitochondria.

CPT1 activity is not changed by diabetes despite the increased protein amount. CPT1 converts long-chain acyl-CoA to acylcarnitines and exists as two isoforms, the muscle (CPT1b) and the liver (CPT1a) isoforms, which

differ with respect to their kinetic properties. The activity of CPT1 was not changed by diabetes in kidney tubule mitochondria (Fig. 2A). The in vivo flux through CPT1 depends on the sensitivity of the enzyme to malonyl-CoA inhibition. Liver mitochondria are significantly less sensitive to malonyl-CoA inhibition (half-maximal inhibitory concentration [IC_{50}] ~5 µmol/L) compared with kidney tubular mitochondria (IC_{50} ~2 µmol/L; Fig. 2B). Figure 2C shows that a slight but significantly higher percentage of CPT I is not inhibited by 2 µmol/L malonyl-CoA (equals the IC_{50} for nondiabetic mitochondria) in diabetic tubule mitochondria compared with the control, suggesting a decrease in the sensitivity of CPT1 to malonyl-CoA in kidney tubules in diabetes.

The two CPT1 isoforms show differences in migration (Fig. 2D), with slightly higher calculated size of CPT1a (~88 kDa) than CPT1b (~82 kDa), as reported (34). CPT1b protein predominates in the heart mitochondria, whereas only CPT1a is present in liver mitochondrial outer membrane. CPT1a is the only isoform expressed in kidney tubule mitochondria, and the amount of CPT1a protein is increased in diabetes.

The activities and amounts of selective FA β-oxidation enzymes are increased in kidney tubules in diabetes. Figure 3A shows the increase in the activity of medium-chain and long-chain acyl-CoA dehydrogenases in tubule mitochondria isolated from the diabetic group. The specific activity of citrate synthase, a mitochondrial marker enzyme, does not differ in tubule mitochondria isolated from the control or diabetic group, indicating that the purity of both preparations was identical. The amounts of CACT and CPT2 proteins are increased in tubule mitochondria isolated from diabetic kidneys compared with controls (Fig. 3B).

Increased capacity of diabetic tubule mitochondria to produce ROS is supported by oxidation of FA substrates; the potential site of electron leakage is located proximal to coenzyme Q within the FA oxidation pathway. When added to intact mitochondria, Amplex red detects the net mitochondrial release of H_2O_2 into the buffer when H_2O_2 production by SOD surpasses its consumption by mitochondrial antioxidant defense mechanisms. Superoxide generated toward and within the mitochondrial matrix is converted to H_2O_2 by the matrix Mn-SOD, whereas the superoxide generated toward the intermembrane space is converted to H_2O_2 by the intermembrane Cu/Zn-SOD.

Surprisingly, control and diabetic tubule mitochondria both produce equal amounts of H_2O_2 when oxidizing pyruvate (Fig. 4A), despite the decreased oxidation of pyruvate in diabetes (Fig. 1). Rotenone (complex I inhibitor that limits the electron flow into complex III) does not additionally increase but rather decreases the release of H_2O_2. The addition of antimycin A has no effect on H_2O_2 in the control or diabetic tubule mitochondria oxidizing pyruvate.

In contrast, diabetic tubule mitochondria oxidizing a FA substrate (Fig. 4B) produce a larger amount of H_2O_2 than the control mitochondria under basal conditions (no inhibitor added). Rotenone does not additionally increase but rather decreases the H_2O_2 production in control and diabetic tubule mitochondria. In contrast, the complex III inhibitor antimycin A significantly increases the production of H_2O_2 in diabetic tubule mitochondria but has no effect on control tubule mitochondria. The data indicate that the maximal capacity (antimycin A-added) of kidney tubule mitochondria oxidizing fat substrates is increased by diabetes; rotenone does not decrease this H_2O_2 maximal

TABLE 2

Oxidative properties of kidney cortical tubule mitochondria isolated from kidneys of control and diabetic rats with glutamate as the substrate

	Control rats $n = 7$	Diabetic rats $n = 6$
State 3	100.0 ± 8.3	$154.0 \pm 12.9*$
State 4	22.0 ± 3.7	20.0 ± 1.6
RCR	5.2 ± 0.7	$8.1 \pm 0.8*$
ADP-to-oxygen ratio	3.1 ± 0.2	3.0 ± 0.2
Maximal ADP	110.0 ± 9.9	$159.0 \pm 12.8*$
Dinitrophenol	80.0 ± 3.8	$128.0 \pm 14.8*$

Data are presented as mean ± SEM. State 3 was induced with 0.2 mmol/L ADP. Respiratory rates are expressed as nA O/min/mg mitochondrial protein. Maximal ADP: State 3 with saturating 2 mmol/L ADP. *$P < 0.05$.
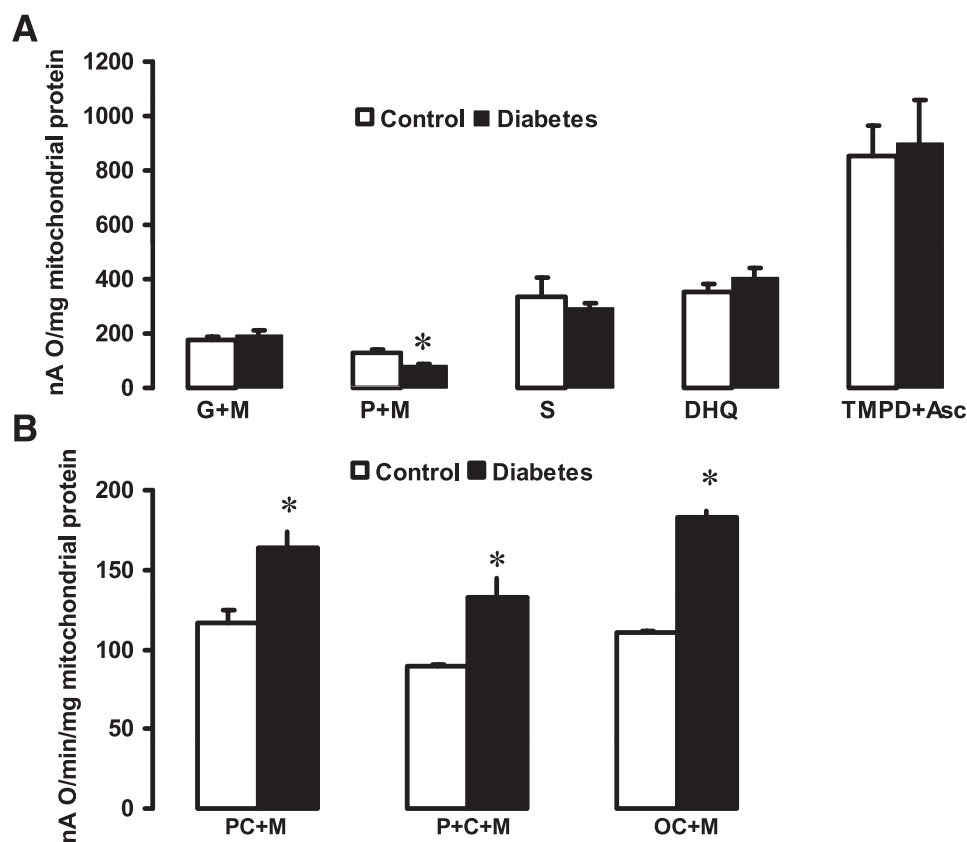
FIG. 1. State 3 respiratory rates of kidney cortical tubule mitochondria. *A:* ETC site-specific substrates. Substrates that donate the reducing equivalents to complex I (G+M, glutamate + malate; P+M, pyruvate + malate), II (S, succinate + rotenone), III (DHQ, DHQ + rotenone), and IV (TMPD+Asc, TMPD + ascorbate + rotenone) were used. *B:* Lipid substrates. PC+M, palmitoylcarnitine + malate; P+C+M, palmitoyl-CoA + carnitine + malate; OC+M, octanoylcarnitine + malate. State 3 was induced with 0.2 mmol/L ADP. *$P < 0.05$ control ($n = 7$) vs. diabetic ($n = 6$). Mean ± SEM.

release capacity with fat substrates. H_2O_2 released by control and diabetic tubule mitochondria oxidizing pyruvate or fat substrate was dissipated by catalase at similar extent, indicating that the increase in the measured fluorescence was because of H_2O_2 and not induced by the chemical reaction of Amplex red with FA hydroperoxides.

When oxidizing succinate at complex II (Fig. 4C), control and diabetic tubule mitochondria both produce H_2O_2, which was decreased in both by ~45% with rotenone, which inhibits the reversed electron transport toward complex I. The data indicate that a major source of superoxide in kidney tubule mitochondria oxidizing succinate is the electron back-flow to complex I and that this feature is unchanged by diabetes. The addition of antimycin A increases the production of H_2O_2 in control and diabetic tubule mitochondria oxidizing succinate.

This increase in the net release of H_2O_2 by diabetic mitochondria with fat substrates indicates that the production surpasses its consumption by mitochondrial antioxidant defense mechanisms. The amount of both SODs determined by immunoblot analysis was not significantly changed by diabetes (Fig. 4D). These data indicate that it is the production of superoxide rather than its dismutation that leads to increased H_2O_2 release in the buffer by diabetic kidney tubule mitochondria.

DISCUSSION

This study shows that 8- to 9-week type 1 diabetes induces an increase in mitochondrial FA β-oxidation without defects

in the electron transport and identifies oxidation of FA rather than glycolysis-derived substrate (pyruvate) oxidation as the source of mitochondrial ROS in diabetic tubules. Because more than 90% of kidney cortex consists of proximal tubules, our results can be attributed to proximal tubule mitochondria. These changes in mitochondria coexist with renal structural and functional modifications consistent with the early stage of DN (35,36).

Diabetic cortical tubule mitochondria reach maximal respiratory rates with glutamate when oxidation is coupled with and depends on phosphorylation of ADP, and do not further increase when the control of oxidation by phosphorylation is eliminated by the uncoupler. These data show that the control site of oxidative phosphorylation is located at the level of glutamate oxidation to form NADH or electron transport rather than at the level of the phosphorylation system. When substrates that donate electrons at specific sites in the ETC were used, no change in respiratory rates was detected, showing that the formation of NADH from glutamate (glutamate transporter or dehydrogenase) rather than the electron transport is increased in diabetes.

The decrease in pyruvate + malate oxidation in diabetic tubule mitochondria suggests a decrease in either pyruvate transporter or pyruvate dehydrogenase that was reported inhibited in the diabetic kidney (15,37). However, the oxidation of pyruvate in isolated tubule mitochondria was performed with a concentration of pyruvate (10 mmol/L) that keeps pyruvate dehydrogenase in its active form
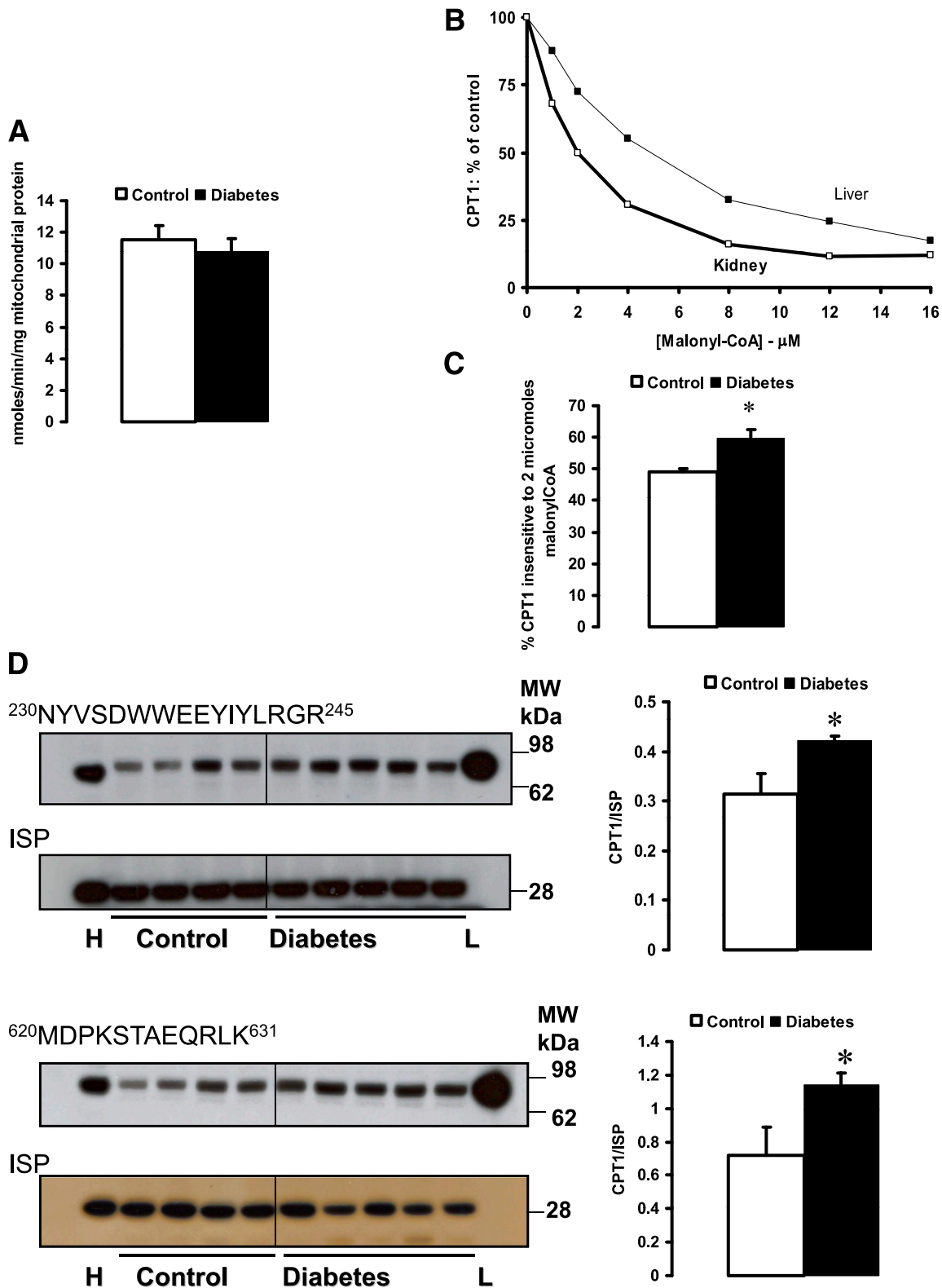
FIG. 2. CPT1 in kidney cortical tubule mitochondria. *A*: Specific activity of CPT1 in tubule mitochondria from control and diabetic kidneys. *B*: Comparison of malonyl-CoA sensitivity (IC$_{50}$) of CPT1 in mitochondria from control rat liver and kidney cortical tubules. *C*: The percentage of CTP1 not inhibited by 2 μmol/L malonyl-CoA in tubule mitochondria from control and diabetic kidneys. *D*: Semiquantitative determination CPT1 protein with antibodies prepared against the amino acid sequence is shown. The bar graphs represent the densitometric quantitation of the immunoblots expressed in arbitrary units normalized per iron sulfur protein (ISP). H, heart subsarcolemmal mitochondria; L, liver mitochondrial outer membrane. *$P < 0.05$ control vs. diabetic. Mean ± SEM. (A high-quality color representation of this figure is available in the online issue.)
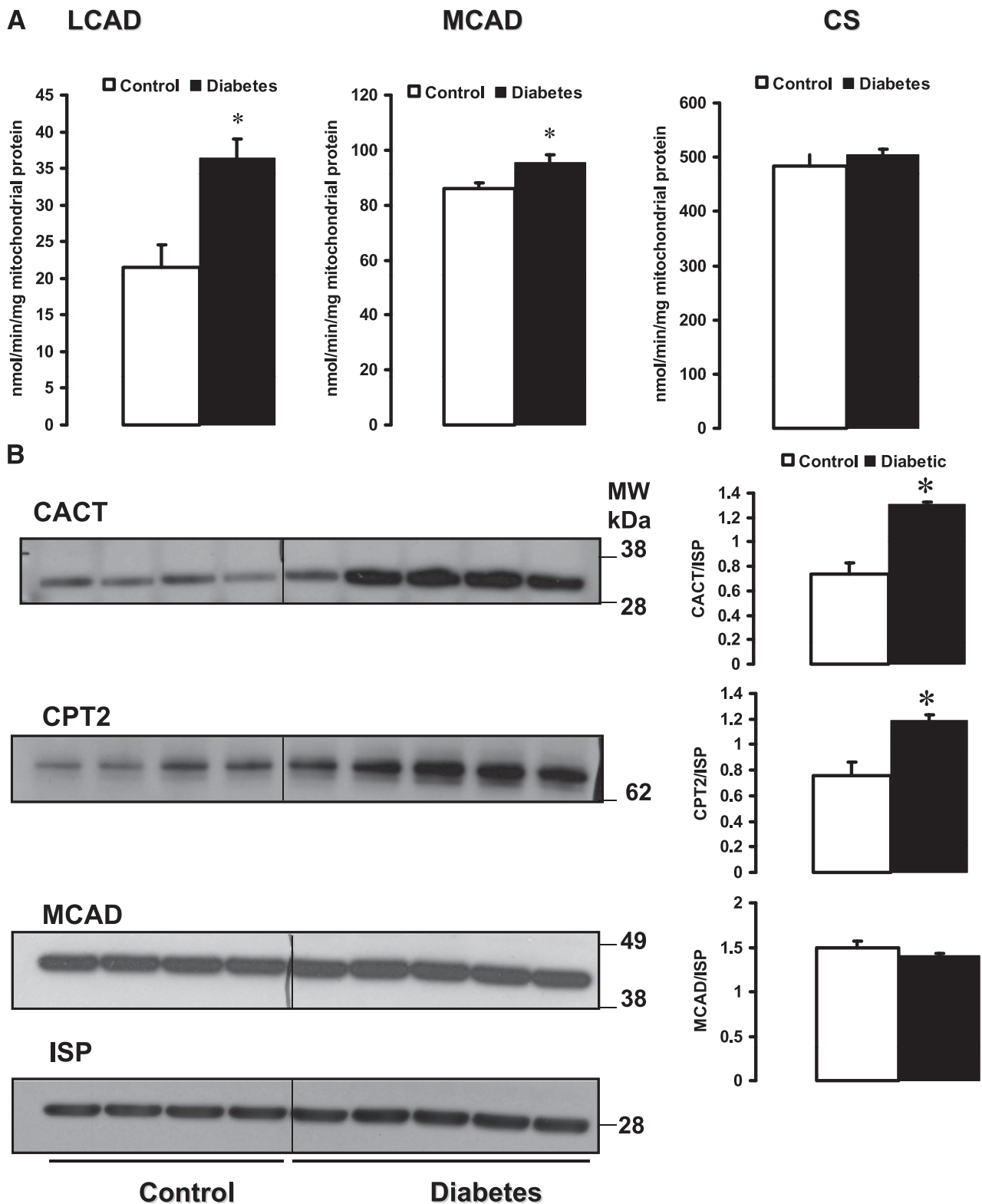
FIG. 3. The specific activities and immunoquantitation of fatty acid β-oxidation enzymes in kidney cortical tubule mitochondria. *A*: Enzyme activities were measured in detergent-solubilized, frozen-thawed mitochondria from control and diabetic rats. CS, citrate synthase. *B*: Immunoblots and densitometric quantitation of the immunoblots are expressed in arbitrary units normalized per iron sulfur protein (ISP). *P < 0.05 control vs. diabetic. Mean ± SEM.

by inhibiting pyruvate kinase (38). Therefore, pyruvate transporter rather than pyruvate dehydrogenase seems to be responsible for the decrease in pyruvate oxidation in diabetic tubule mitochondria.

Diabetic tubule mitochondria oxidize FA substrates at higher rates than the controls. This is associated with an increase in the specific activities of both MCAD and LCAD without changes in the MCAD amount, suggesting
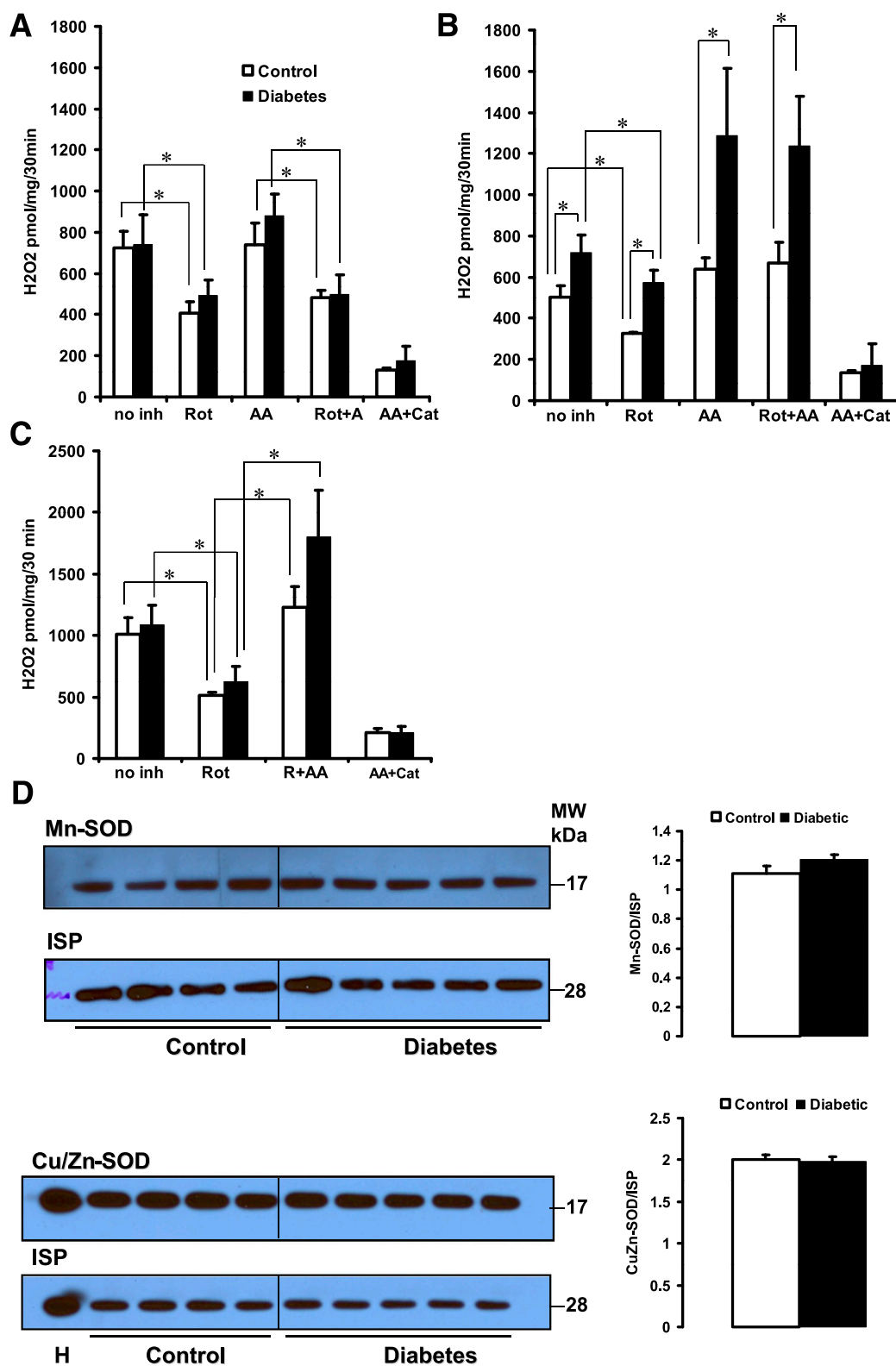
FIG. 4. Kidney cortical tubule mitochondria production of H_2O_2 with pyruvate + malate (*A*) palmitoylcarnitine + malate (*B*), and succinate + rotenone (*C*) as the substrates. Rot, rotenone; AA, antimycin A; Cat, catalase. *D*: Semiquantitative determination of mitochondrial Mn-SOD and Cu/Zn-SOD. The bar graphs represent the densitometric quantitation of the immunoblots expressed in arbitrary units normalized per iron sulfur protein (ISP). H, heart subsarcolemmal mitochondria. *$P < 0.05$ compared with the indicated groups. Mean ± SEM. (A high-quality color representation of this figure is available in the online issue.)

post-translational modifications that stimulate its catalytic activity. In contrast, despite the increase in CPT1a protein amount that favors mitochondrial FA β-oxidation, the catalytic activity of CTP1a is unchanged in diabetes, suggesting that CPT1 has a low flux control coefficient for mitochondrial FA β-oxidation in kidney tubules in diabetes.

The twofold higher IC_{50} for malonyl-CoA of CPT1 assessed in control tubule mitochondria compared with liver mitochondria is not due to the presence of the CPT1b isoform, as shown by the Western blot approach. We propose that this kinetic property of CPT1a is an intrinsic feature of this isoform in kidney tubule mitochondria due to differences in outer membrane lipid environment or to post-translational modifications.

Proximal kidney tubules (>90% of the kidney cortex) rely on FA rather than glucose to form ATP during normal metabolic conditions (14); we found that this feature is enhanced in diabetes. Peroxisome proliferator-activated receptors (PPAR) are potential candidates that induce the enhanced mitochondrial FA β-oxidation in kidney tubules in diabetes. All members of this subfamily of nuclear receptors were detected in kidney cortex (39), are activated by NEFA (40), which were found increased in the diabetic sera in our model (Table 1), induce expression of FA β-oxidation enzymes (41), and promote FA utilization.

Our data also show that diabetic tubule mitochondria produce more ROS than the controls under both basal and maximal conditions when oxidizing FA substrates compared with oxidation of pyruvate. Prior reports suggesting that pyruvate may be the source of ROS (42) were based on the association of the elevated inner membrane potential and ROS with the increased content of both pyruvate and the tricarboxylic cycle intermediates originating from the pyruvate carboxylase route in mitochondria isolated from the whole kidney tissue. Our results contradict this assumption. Owing to kidney cellular complexity, the current study was performed specifically on mitochondria isolated from cortical tubular structures (highly oxidative nephron segments that depend on the ATP generated from FA oxidation) free of medullary structures (highly glycolytic). The inhibition of the pyruvate dehydrogenase in the diabetic medulla may lead to the increased content of pyruvate within mitochondria isolated from the whole kidney.

Oxidation of FA substrates was reported to be a source of ROS in the normal heart (43) and skeletal muscle (44) mitochondria. Increased oxidation of FA in aortic endothelial cells was reported to increase superoxide production from sites located within the electron transport (45,46). Fatty acids are complex I and III substrates via NADH and $FADH_2$–ETF/ETF-QOR, respectively (Fig. 5). Rotenone blocks the distal part of complex I, increases the reduction of the NADH dehydrogenase site of complex I, and causes an electron leak toward the matrix in cardiac mitochondria (33,43). Because rotenone does not increase H_2O_2 production with lipid and nonlipid complex I substrates in control and diabetic tubule mitochondria, we propose that complex I is not the main site of ROS production in tubule mitochondria or that complex I–generated oxidants are directed toward the mitochondrial matrix and inactivated by matrix-antioxidant systems in both control and diabetic states. The equal decrease of ROS with rotenone indicates that an additional site rather than the reverse electron transport to complex I is responsible for the increased ROS generation by diabetic tubule mitochondria oxidizing fat substrates.

Complex III is a key site for ROS generation in cardiac mitochondria (33,43). Because the limitation of the electron flow from complex I into complex III with rotenone equally decreased the release of H_2O_2 by control and diabetic mitochondria oxidizing pyruvate, the data show that complex III is the sole contributor to the release of H_2O_2 by tubular mitochondria oxidizing pyruvate. In contrast with cultured cells (45,46), the rotenone-inhibited tubule mitochondria from diabetic kidney show a higher amount of H_2O_2 than the control mitochondria oxidizing fat substrates. These data also indicate that a site other than complex III significantly contributes to ROS generation when fatty acids are used as substrates in diabetes.

The ubiquinol oxidation (Qo) site in complex III is the main site of electron leak oriented equally toward the intermembrane space and mitochondrial matrix (47). Antimycin A binds to complex III at a site that overlaps the ubiquinone reduction (Qi) site, increases electron leak from the Qo site, and increases superoxide generation. The minimal increase in H_2O_2 production in control mitochondria with antimycin A indicates that the superoxide production is oriented mainly toward the matrix and scavenged by the matrix antioxidants. The different topology of the superoxide released by kidney tubule mitochondria compared with cardiac mitochondria may reside in differences in lipid structure of the inner membrane responsible for a different mobility of the semiquinone in the Q cycle.

Antimycin A increases H_2O_2 released by diabetic tubule mitochondria oxidizing only fat substrates, indicating that major changes in the topology of ROS production are induced by diabetes in kidney tubule mitochondria when oxidizing fat. With succinate + rotenone + antimycin, diabetic tubule mitochondria do not show a significantly higher maximal capacity to produce H_2O_2 compared with the control mitochondria ($P = 0.081$). Because complex II is not considered to be the major site of superoxide production, the data suggest that the maximal capacity of the Qo site in complex III to generate oxidants does not differ between the control and diabetic tubule mitochondria.

A more likely explanation is that an additional site within the ETF/ETF-QOR–Qo segment (Fig. 5) becomes a site of superoxide production. The first dehydrogenase reaction in FA β-oxidation generates $FADH_2$, with the electron donated to ETF. The FAD prosthetic group of ETF is rapidly reduced to the semiquinone form and more slowly to the fully reduced form (48,49), suggesting that the semiquinone form of the ETF may be the electron donor for the univalent reduction of oxygen to form superoxide. Similarly, the FAD prosthetic group of ETF-QOR cycles between the oxidized and partially reduced (semiquinone) forms. However, crystallography studies of ETF-QOR show that the semiquinone is protected from reacting with molecular oxygen (50) and that ETF-QOR is unlikely to be a site of superoxide production. Specific inhibitors must be developed to evaluate the real contribution of ETF or ETF-QOR to oxyradical production.

The matrix-generated superoxide from the site located at the ETF is dismutated to H_2O_2 by the matrix Mn-SOD. This enzyme reroutes superoxide from combining with nitric oxide to form peroxynitrite, which may alter mitochondrial function via tyrosine nitration of the ETC protein subunits. Therefore, the fate of mitochondrial ETC in long-term diabetes is controlled by crosstalk between mitochondrial antioxidant defense mechanisms.
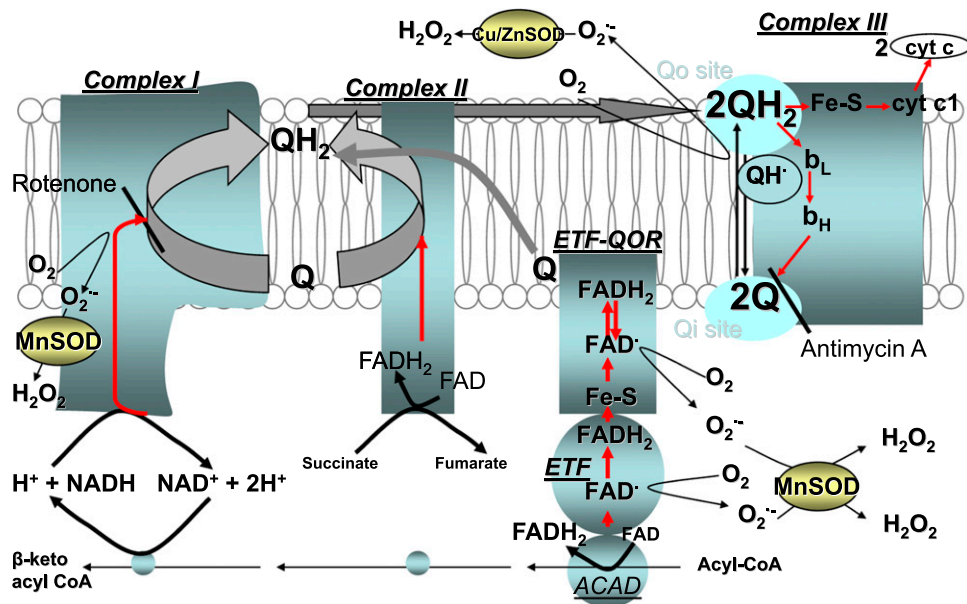
FIG. 5. The passage of electrons from FA to the ETC. Sites of electron leak and superoxide production and its dismutation to H_2O_2 are shown. The electron passage is shown in red. Electrons are released by substrate oxidation and captured by NADH and $FADH_2$, which are oxidized by complexes I and II, respectively. These complexes pass the electrons to ubiquinone (Q). The reduced Q (ubiquinol, QH_2) diffuses to and binds within the QH_2 oxidation site (Qo) in complex III (formed by cytochrome b and the Fe-S protein rotated toward it). ETF linked to ETF-QOR provides an alternative pathway to pass electrons to the ETC. The FAD cofactors in ETF and ETF-QOR carry 1 electron at a time with the formation of intermediate semiquinone state of flavin. Flavin in the ETF is rapidly reduced by one electron by acyl-CoA dehydrogenases (ACAD). The slow complete reduction of flavin facilitates the accumulation of semiquinone. The electrons are donated sequentially to the Fe-S center and flavin in the ETF-QOR. Both electrons are further donated to Q (bound to the ETF-QOR in the mitochondrial inner membrane). The QH_2 product leaves this site and is reoxidized in the Qo center of complex III. The transfer of electrons diverges within the Qo site: one electron is transferred to the Fe-S, followed immediately by the other electron transfer to the Qi (Q reduction site) via cytochrome b_L. Under conditions of uninhibited electron flow through complex III, the reaction is rapid, preventing the accumulation of semiquinone ($QH^{\cdot}$) in the Qo site. Antimycin A, a Qi site inhibitor, prevents the electron from leaving complex III, leading to accumulation of $QH^{\cdot}$ and $O_2^{\cdot}$ formation. Rotenone, an inhibitor of the Q reduction site in complex I, prevents the electrons from leaving complex I and reaching complex III, leading to an increase in $O_2^{\cdot}$ formation from complex I toward the matrix and decrease in $O_2^{\cdot}$ formation from Qo in complex III toward the intermembrane space. Superoxide is dismutated by the matrix Mn-SOD and intermembrane space Cu/Zn-SOD. (A high-quality color representation of this figure is available in the online issue.)

In conclusion, mitochondrial ETC is neither the target nor the ROS-generating site in short-term diabetes. This study identifies FA as the source of reducing equivalents responsible for increased ROS production by kidney tubule mitochondria in diabetes and shows that ETF is the major site of electron leakage. A future time course study will help to link the increase in ROS production originating from mitochondrial FA oxidation pathway with the ETC damage and the progression to advanced stages of diabetic kidney disease.

REFERENCES

1. USRDS. USRDS: the United States Renal Data System. Am J Kidney Dis 2003;42(6 Suppl. 5):1–230
2. Spencer MW, Mühlfeld AS, Segerer S, et al. Hyperglycemia and hyperlipidemia act synergistically to induce renal disease in LDL receptor-deficient BALB mice. Am J Nephrol 2004;24:20–31
3. Kambham N, Markowitz GS, Valeri AM, Lin J, D'Agati VD. Obesity-related glomerulopathy: an emerging epidemic. Kidney Int 2001;59:1498–1509
4. Sun L, Halaihel N, Zhang W, Rogers T, Levi M. Role of sterol regulatory element-binding protein 1 in regulation of renal lipid metabolism and glomerulosclerosis in diabetes mellitus. J Biol Chem 2002;277:18919–18927
5. Proctor G, Jiang T, Iwahashi M, Wang Z, Li J, Levi M. Regulation of renal fatty acid and cholesterol metabolism, inflammation, and fibrosis in Akita and OVE26 mice with type 1 diabetes. Diabetes 2006;55:2502–2509
6. Fried LF, Orchard TJ, Kasiske BL. Effect of lipid reduction on the progression of renal disease: a meta-analysis. Kidney Int 2001;59:260–269
7. Nakamura T, Kawagoe Y, Ogawa H, et al. Effect of low-density lipoprotein apheresis on urinary protein and podocyte excretion in patients with nephrotic syndrome due to diabetic nephropathy. Am J Kidney Dis 2005;45:48–53
8. Lane PH, Steffes MW, Fioretto P, Mauer SM. Renal interstitial expansion in insulin-dependent diabetes mellitus. Kidney Int 1993;43:661–667
9. White KE, Bilous RW. Type 2 diabetic patients with nephropathy show structural-functional relationships that are similar to type 1 disease. J Am Soc Nephrol 2000;11:1667–1673

10. Bohle A, Wehrmann M, Bogenschütz O, Batz C, Müller CA, Müller GA. The pathogenesis of chronic renal failure in diabetic nephropathy. Investigation of 488 cases of diabetic glomerulosclerosis. Pathol Res Pract 1991;187:251–259

11. Susztak K, Ciccone E, McCue P, Sharma K, Böttinger EP. Multiple metabolic hits converge on CD36 as novel mediator of tubular epithelial apoptosis in diabetic nephropathy. PLoS Med 2005;2:e45

12. Thomas ME, Morrison AR, Schreiner GF. Metabolic effects of fatty acid-bearing albumin on a proximal tubule cell line. Am J Physiol 1995;268: F1177–F1184

13. Ghiggeri GM, Ginevri F, Candiano G, et al. Characterization of cationic albumin in minimal change nephropathy. Kidney Int 1987;32:547–553

14. Guder WG, Wagner S, Wirthensohn G. Metabolic fuels along the nephron: pathways and intracellular mechanisms of interaction. Kidney Int 1986;29: 41–45

15. Guder WG, Schmolke M, Wirthensohn G. Carbohydrate and lipid metabolism of the renal tubule in diabetes mellitus. Eur J Clin Chem Clin Biochem 1992;30:669–674

16. Huang C, Kim Y, Caramori ML, et al. Diabetic nephropathy is associated with gene expression levels of oxidative phosphorylation and related pathways. Diabetes 2006;55:1826–1831

17. Brownlee M. The pathobiology of diabetic complications: a unifying mechanism. Diabetes 2005;54:1615–1625

18. Nishikawa T, Edelstein D, Du XL, et al. Normalizing mitochondrial superoxide production blocks three pathways of hyperglycaemic damage. Nature 2000;404:787–790

19. Du Y, Miller CM, Kern TS. Hyperglycemia increases mitochondrial superoxide in retina and retinal cells. Free Radic Biol Med 2003;35:1491–1499

20. Coppey LJ, Gellett JS, Davidson EP, Yorek MA. Preventing superoxide formation in epineurial arterioles of the sciatic nerve from diabetic rats restores endothelium-dependent vasodilation. Free Radic Res 2003;37:33–40

21. Lashin OM, Szweda PA, Szweda LI, Romani AM. Decreased complex II respiration and HNE-modified SDH subunit in diabetic heart. Free Radic Biol Med 2006;40:886–896

22. Chacko BK, Reily C, Srivastava A, et al. Prevention of diabetic nephropathy in Ins2(+/)⁻(AkitaJ) mice by the mitochondria-targeted therapy MitoQ. Biochem J 2010;432:9–19

23. Akude E, Zherebitskaya E, Chowdhury SK, Smith DR, Dobrowsky RT, Fernyhough P. Diminished superoxide generation is associated with respiratory chain dysfunction and changes in the mitochondrial proteome of sensory neurons from diabetic rats. Diabetes 2011;60:288–297

24. Bederman IR, Foy S, Chandramouli V, Alexander JC, Previs SF. Triglyceride synthesis in epididymal adipose tissue: contribution of glucose and non-glucose carbon sources. J Biol Chem 2009;284:6101–6108

25. Kreisberg JI, Hoover RL, Karnovsky MJ. Isolation and characterization of rat glomerular epithelial cells in vitro. Kidney Int 1978;14:21–30

26. Rosca MG, Mustata TG, Kinter MT, et al. Glycation of mitochondrial proteins from diabetic rat kidney is associated with excess superoxide formation. Am J Physiol Renal Physiol 2005;289:F420–F430

27. Hoppel C, DiMarco JP, Tandler B. Riboflavin and rat hepatic cell structure and function. Mitochondrial oxidative metabolism in deficiency states. J Biol Chem 1979;254:4164–4170

28. Chance B, Williams GR. Respiratory enzymes in oxidative phosphorylation. III. The steady state. J Biol Chem 1955;217:409–427

29. Hoppel CL, Kerner J, Turkaly P, Turkaly J, Tandler B. The malonyl-CoA-sensitive form of carnitine palmitoyltransferase is not localized exclusively in the outer membrane of rat liver mitochondria. J Biol Chem 1998;273: 23495–23503

30. Distler AM, Kerner J, Lee K, Hoppel CL. Post-translational modifications of mitochondrial outer membrane proteins. Methods Enzymol 2009;457: 97–115

31. Hoppel C, Kerner J, Turkaly P, Tandler B. Rat liver mitochondrial contact sites and carnitine palmitoyltransferase-I. Arch Biochem Biophys 2001;392: 321–325

32. Bugger H, Chen D, Riehle C, et al. Tissue-specific remodeling of the mitochondrial proteome in type 1 diabetic akita mice. Diabetes 2009;58: 1986–1997

33. Chen Q, Vazquez EJ, Moghaddas S, Hoppel CL, Lesnefsky EJ. Production of reactive oxygen species by mitochondria: central role of complex III. J Biol Chem 2003;278:36027–36031

34. McGarry JD, Brown NF. The mitochondrial carnitine palmitoyltransferase system. From concept to molecular analysis. Eur J Biochem 1997;244:1–14

35. Liu CX, Hu Q, Wang Y, et al. Angiotensin-converting enzyme (ACE) 2 overexpression ameliorates glomerular injury in a rat model of diabetic nephropathy: a comparison with ACE inhibition. Mol Med 2011;17:59–69

36. Sato Y, Feng GG, Huang L, et al. Enhanced expression of naofen in kidney of streptozotocin-induced diabetic rats: possible correlation to apoptosis of tubular epithelial cells. Clin Exp Nephrol 2010;14:205–212

37. Huang B, Wu P, Popov KM, Harris RA. Starvation and diabetes reduce the amount of pyruvate dehydrogenase phosphatase in rat heart and kidney. Diabetes 2003;52:1371–1376

38. Chiang PK, Sacktor B. Control of pyruvate dehydrogenase activity in intact cardiac mitochondria. Regulation of the inactivation and activation of the dehydrogenase. J Biol Chem 1975;250:3399–3408

39. Wang YX. PPARs: diverse regulators in energy metabolism and metabolic diseases. Cell Res 2010;20:124–137

40. Bensinger SJ, Tontonoz P. Integration of metabolism and inflammation by lipid-activated nuclear receptors. Nature 2008;454:470–477

41. Ouali F, Djouadi F, Merlet-Bénichou C, Bastin J. Dietary lipids regulate beta-oxidation enzyme gene expression in the developing rat kidney. Am J Physiol 1998;275:F777–F784

42. de Cavanagh EM, Ferder L, Toblli JE, et al. Renal mitochondrial impairment is attenuated by AT1 blockade in experimental Type I diabetes. Am J Physiol Heart Circ Physiol 2008;294:H456–H465

43. St-Pierre J, Buckingham JA, Roebuck SJ, Brand MD. Topology of superoxide production from different sites in the mitochondrial electron transport chain. J Biol Chem 2002;277:44784–44790

44. Seifert EL, Estey C, Xuan JY, Harper ME. Electron transport chain-dependent and -independent mechanisms of mitochondrial H_2O_2 emission during long-chain fatty acid oxidation. J Biol Chem 2010;285:5748–5758

45. Du X, Edelstein D, Obici S, Higham N, Zou MH, Brownlee M. Insulin resistance reduces arterial prostacyclin synthase and eNOS activities by increasing endothelial fatty acid oxidation. J Clin Invest 2006;116:1071–1080

46. Yamagishi SI, Edelstein D, Du XL, Kaneda Y, Guzmán M, Brownlee M. Leptin induces mitochondrial superoxide production and monocyte chemoattractant protein-1 expression in aortic endothelial cells by increasing fatty acid oxidation via protein kinase A. J Biol Chem 2001;276:25096–25100

47. Muller FL, Liu Y, Van Remmen H. Complex III releases superoxide to both sides of the inner mitochondrial membrane. J Biol Chem 2004;279:49064–49073

48. Hall CL, Lambeth JD. Studies on electron transfer from general acyl-CoA dehydrogenase to electron transfer flavoprotein. J Biol Chem 1980;255: 3591–3595

49. Steenkamp DJ, Husain M. The effect of tetrahydrofolate on the reduction of electron transfer flavoprotein by sarcosine and dimethylglycine dehydrogenases. Biochem J 1982;203:707–715

50. Zhang J, Frerman FE, Kim JJ. Structure of electron transfer flavoprotein-ubiquinone oxidoreductase and electron transfer to the mitochondrial ubiquinone pool. Proc Natl Acad Sci USA 2006;103:16212–16217